mater.scichina.com link.springer.com

Published online 11 June 2024 | https://doi.org/10.1007/s40843-023-2912-5
Sci China Mater 2024, 67(7): 2266–2276

Self-assembled electrode-electrolyte interphase enabling highly reversible Zn metal anode for aqueous zinc batteries

Qibin Shen[†], Taiqiang Chen[†], Xin Li, Shuixin Xia, Tao Yuan, Yuepeng Pang and Shiyou Zheng[*]

ABSTRACT **The cycle life of aqueous zinc batteries is hindered by undesired side reactions and dendrite growth of the Zn metal anode due to the lack of an advanced solid electrolyte interphase. Here, a pioneering self-assembled electrode-electrolyte interphase (AEEI) constructed from electrolyte additives of amphiphilic molecules (APMs) is presented. Specifically, polyvinyl pyrrolidone (PVP) molecules are demonstrated due to their high electron-donating property of the carbonyl oxygen atoms in pyrrolidone groups that conjugate with aromatic pyrrole rings. The formation and stability of this interphase is fundamentally prompted by the interaction between the carbonyl oxygen atoms of APMs and Zn metal as well as Zn^{2+} ions, which is elucidated by X-ray photoelectron spectroscopy and Fourier transform infrared spectroscopy. The resultant AEEI predominantly consists of a dense lamellar micelle of APMs enriched with Zn^{2+} ions. Maintaining the contents of APMs above a critical aggregation concentration of ~0.1% within the electrolyte guarantees the inherent stability of the AEEI, avoiding concerns of crack formation or detachment. Conformal and dendrite-free Zn deposition is achieved with the help of the AEEI, benefitting from its ability to suppress water decomposition side reactions and unfavorable 2D diffusion of Zn^{2+} ions. The AEEI ensures a long cycle life of more than 2000 h for symmetric Zn cells, Coulombic efficiency of >99.2% over 500 cycles for Zn||Ti cells, and a capacity retention of 76% over 500 cycles for V_2O_5|| Zn full cells in 1 M $Zn(OTf)_2$ electrolyte with 1% PVP.**

Keywords: aqueous zinc batteries, zinc metal anode, electrode-electrolyte interphase, self-assembly

INTRODUCTION

Recently, mild aqueous Zn batteries using Zn metal as the anode have attracted extensive research interests due to the advantages of low cost and high energy density, as Zn metal shows a high capacity of 819 mA h g^{-1} and a redox potential of −0.76 V *versus* a standard hydrogen electrode (SHE) [1–4]. The low redox potential of Zn metal *vs.* SHE ensures a high working voltage of the full cell and, as a result, a high energy density [5–8]. However, this intrinsically sacrifices the thermodynamic stability of Zn metal in aqueous electrolyte and leads to the hardly inevitable hydrogen evolution reaction (HER) during Zn deposition. The Zn anode surface is corroded, generating by-products such as $Zn(OH)_2$ and ZnO, because of a sharp increase in local pH resulting from HER [9–11]. The resultant rough and inhomogeneous morphology of the Zn anode surface due to corrosion can accelerate dendrite growth during Zn deposition [12–16]. The problems of HER side reaction and Zn dendrite significantly restrict the Coulombic efficiency (CE) and cycle life of the Zn metal anode.

To handle these problems, intensive research efforts have been made, such as construction of a composite anode [17], design of the electrolyte [18], modification of the anode-electrolyte interface [19] and design of the separator [20], among which the anode-electrolyte interface is considered crucial [21]. Artificial solid electrolyte interphase (SEI) on the Zn surface blocks the anode from direct contacting with water and permits transportation of Zn^{2+} ions. Artificial SEIs such as inorganic [22,23], polymer [24,25] and metal organic framework-based films [26–28] have been reported to suppress water decomposition and Zn dendrite growth. Large volume changes during repeated cycles of the Zn anode result in degradation and failure of these interphase due to the lack of self-reparable capability [29]. *In situ* formation of SEI *via* electrolyte decomposition on the electrode surface is regarded as a promising route to overcome this drawback resembling that in lithium ion batteries. However, reduction of the aqueous solvent produces harmful H_2 gas instead of passivating interphase. Common anions as well as organic solvents or additives are difficult to decompose reductively before Zn deposition, because the redox potential of Zn metal (−0.76 V *vs.* SHE) is much higher than that of Li metal (−3.04 V *vs.* SHE) [30,31]. Accordingly, regulating the solvation structure of Zn^{2+} cation *via* water-in-salt [32], eutectic liquid [33] or mixed organic solvent [34,35] has been reported to upshift the redox potentials of the electrolyte components. This facilitates the reduction of Zn^{2+} coordinated anions (typically fluorine-containing) prior to Zn deposition, resulting in the *in-situ* formation of ZnF_2-based SEI. But the solvation structure strategy typically relies on an extreme high concentration of salt or organic solvent and, thus, intrinsically suffers from drawbacks of high cost and/or high viscosity.

The *in-situ* construction of an interphase on the Zn anode in low concentration aqueous electrolyte is necessary. Up to now, this remains a great challenge and only a few successful attempts have been realized. Taking advantage of the local alkaline conditions near the Zn surface from HER, electrolyte additives of $Zn(NO_3)_2$ [9] and $Zn(H_2PO_4)_2$ [29] are reported to *in situ* be converted to SEI mainly composed of $Zn_5(CO_3)_2(OH)_6$ and $Zn_3(PO_4)_2{\cdot}4H_2O$, respectively, which enable high CE and dendrite-

School of Materials and Chemistry, University of Shanghai for Science and Technology, Shanghai 200093, China
[†] These authors contributed equally to this work.
[*] Corresponding author (email: syzheng@usst.edu.cn)

free Zn deposition. Based on a similar mechanism, an *in situ* formed $ZnCO_3$ SEI was presented by Zhu *et al.* [36] *via* purging CO_2 gas into the electrolyte. Meanwhile, a few specially screened and designed additives such as $Me_3EtNOTF$ [37] and sulfanilamide [38] have been demonstrated to decompose reductively on the Zn metal surface and form robust, Zn^{2+}-conducting and waterproof SEI. Moreover, an alternative salt of zinc sulfamate ($Zn(NH_2SO_3)_2$) was proposed by Xu *et al.* [39] to form a stable SEI mainly composed of ZnS, $ZnSO_3$, and $ZnCO_3$. It was found that the sulfamate anions were favorably adsorbed on the Zn anode and constructed an anion-rich Helmholtz plane, promoting their preferential electroreduction. However, most of the reported SEI mainly comprises of inorganics such as zinc basic salt, ZnF_2, $ZnSO_3$, and $ZnCO_3$, and few organics or polymers are included, considering the rather high redox potential of Zn metal. It results in a rather brittle interphase with high risk of cracks and even peeling off from the Zn surface because of large volume change or gas blowing from HER. Innovative Zn metal electrode-electrolyte interphase with inherent properties of interface distribution and flexibility is highly desired.

Herein, a pioneering self-assemble process grounded in the self-assembly of amphiphilic molecules (APMs) was designed to construct a self-assembled electrode-electrolyte interphase (AEEI) on Zn metal. APMs with hydrophilic pyrrolidone groups were selected using polyvinyl pyrrolidone (PVP) as a demonstration due to the high electron-donating property of carbonyl oxygen atoms that conjugate with aromatic pyrrole rings. The formation and stability of the AEEI are fundamentally guaranteed by the interaction between the carbonyl oxygen atoms of the APMs and Zn metal as well as Zn^{2+} ions. The resultant AEEI predominantly consists of a dense lamellar micelle of APMs with abundant Zn^{2+} ions. Moreover, its structure and stability are intrinsically governed by the concentration of APMs in the electrolyte. As long as the concentration remains above a critical aggregation concentration (CAC) (~0.1%), this AEEI is spontaneously self-assembled at the electrode-electrolyte interface, avoiding the risk of cracks or detachment. Importantly, the AEEI can block Zn metal from direct contacting with active H_2O and suppress the side reactions. The AEEI also impedes unfavorable two-dimensional (2D) diffusion and facilitates conformal Zn deposition, benefiting from the reduced interfacial energy and the coordination between carbonyl oxygen atoms and Zn^{2+} ions. Accordingly, exceptional long-term cycling stability (>2000 h) in Zn||Zn symmetric cell and high reversibility (CE > 99.2% over 500 cycles) in Zn||Ti cell are achieved in 1 M zinc trifluoromethanesulfonate ($Zn(OTf)_2$) electrolyte with 1% PVP. Furthermore, remarkable capacity retention of 76% after 500 cycles is attained by a V_2O_5||Zn full cell in electrolyte with 1% PVP, outperforming the value of 42% in the electrolyte without PVP.

EXPERIMENTAL SECTION

Zn foil (>99.9%, 100 μm), Cu foil (>99.9%, 30 μm), and Ti foil (>99.9%, 30 μm) were purchased from Tengfeng metal material Co., Ltd. $Zn(OTf)_2$ and PVP (average MW: 8000 g mol^{-1}) were purchased from Sigma-Aldrich Corporation. Battery grade V_2O_5 powder was received from MTI Corporation. Aqueous electrolytes with APMs were prepared by adding 0.1, 1 and 5% (weight ratio) PVP powder into 1 M $Zn(OTf)_2$ aqueous solutions. The solution was stirred at room temperature for 10 min until PVP was completely dissolved. The electrolytes with 0.01% and 0.001% PVP were prepared *via* diluting the 0.1% PVP solution with the prepared 1 M $Zn(OTf)_2$ aqueous solutions. V_2O_5 electrode slurry was prepared by homogeneously mixing V_2O_5, Super-P, and poly(vinylidene fluoride) (PVDF) at a weight ratio of 8:1:1 in *N*-methyl-2-pyrrolidone (NMP) solvent. The electrode slurry was coated onto Ti foil, and then dried in a vacuum oven at 80°C for 10 h to make the cathode. The typical loading mass of V_2O_5 is ~2.5 mg cm^{-2}.

The morphology of the Zn anode was investigated using field emission scanning electron microscopy (FESEM, JEOL JSM-7500F). X-ray diffraction (XRD) was conducted on a Rigaku MiniFlex600 with Cu Kα radiation between 5° and 70° at a scan rate of 2° min^{-1}. X-ray photoelectron spectroscopy (XPS) was performed using an X-ray photoelectron spectrometer (ESCALAB MK II) with a monochromatic Al Ka source. Fourier transform infrared spectra (FTIR) were recorded on a Cary 630 (Agilent) spectrometer in the attenuated total reflectance (ATR) module with 32 scans per measurement. *In situ* optical observations were conducted on an optical microscope (OM, Olympus BX43), employing a homemade optical cell with a quartz window, where two Zn metal electrodes (1-cm width, 1-cm length, and 100-μm thickness) acted as the working and counter electrodes, respectively. The contact angles of electrolytes on the Zn foil were measured on an optical contact angle system (Dataphysics OCA 25) with a 3 μL of electrolyte droplet at 25°C.

Zn||Zn symmetrical coin cells were assembled using Zn foil as both the working and counter electrodes, and glass fiber (Whatman, GFA, with a thickness of 0.68 mm and a pore size of 1 μm) as the separator. The symmetrical coin cells were cycled at 1, 2, and 5 mA cm^{-2} with a capacity of 1 mA h cm^{-2} for long-term cycling. Ti||Zn coin cells were assembled to evaluate the CE of Zn metal anode with Ti foil as the working electrode, Zn foil as the counter and reference electrodes, and GFA glass fiber as the separator. The Ti||Zn cells were cycled at 1 mA cm^{-2} with a discharge capacity of 1 mA h cm^{-2} and a charging cutoff voltage of 0.5 V. V_2O_5||Zn coin cells were assembled using V_2O_5 as the working electrode and Zn metal as the counter and reference electrodes. The charge/discharge voltage range for V_2O_5||Zn cells was 0.3–1.6 V and the cells were cycled at 0.2 A g^{-1} for 10 formation cycles before long-term cycling at 2 A g^{-1}. All the galvanostatic charge-discharge cycles were conducted using a LANHE battery tester (Wuhan). The interface impedances of the Zn metal anode in various electrolytes were analyzed by electrochemical impedance spectroscopy (EIS) that was conducted using a Gamry Potentiostat (Reference 600) in a three-electrode configuration with two Zn metal electrode as the working and counter electrodes, and Ag/AgCl as the reference electrode, at a frequency range from 10^6 to 10^{-1} Hz with an AC amplitude of 10 mV. Linear sweep voltammetry (LSV) was recorded using an electrochemical work station (CHI660E) in a three-electrode configuration using Ag/AgCl as the reference electrode at a scan rate of 0.1 mV s^{-1}. Chronoamperograms were conducted using CHI660E with a −200 mV overpotential. Exchange current densities were measured by fitting Tafel plots for Zn||Zn symmetric coin cells at a scan rate of 1 mV s^{-1} in a voltage range of −1.2 to −0.8 V *vs.* Ag/AgCl (conducted using CHI660E).

RESULTS AND DISCUSSION

AEEI

The Zn metal electrode-electrolyte interphase was self-assembled

from electrolyte additives of APMs in 1 M $Zn(OTf)_2$ aqueous electrolyte using PVP as a demonstration. PVP molecules have amphiphilic structures with hydrophilic pyrrolidone groups. A pyrrolidone group consists of an aromatic pyrrole ring conjugated with a carbonyl oxygen at the α position, resulting in high electron-donating property of the carbonyl oxygen. It is well known that the surfaces of the metal and metal oxide are generally hydrophilic [40–42]. There is a driving force (which will be discussed later) for PVP APMs to adsorb on the hydrophilic Zn metal surface, orienting their hydrophilic groups (i.e., the carbonyl groups) at the solid interface and the hydrophobic hydrocarbon chain pointing to the electrolyte solution to reduce the free energy [40]. The concentration of APMs is the crucial factor that affects the adsorption processes. Fig. 1a schematically illustrates the influence of concentration on the adsorption and assembly of APMs at the metal-electrolyte interface, rooted in the widely accepted chemistry of surfactants [40,41,43,44]. At low concentrations, minimal adsorption of APMs occurs on the substrate. As the concentration reaches an intermediate level, APMs begin to aggregate on the substrate, albeit in a loosely distributed manner. Around the CAC, a uniform and porous film of adsorbed APMs forms on the substrate. A lamellar micelle of two or multiple layers of APMs, with the hydrophilic/hydrophobic heads facing outward towards each other to minimize the free energy, will finally be constructed, forming the framework of AEEI if sufficient additives of APMs are present in the electrolyte.

The impact of as-formed AEEI on the electrochemical behavior of the Zn metal anode was investigated using EIS and LSV [45,46] to reveal the evolution of interface impedance of Zn metal electrode and Zn deposition nucleation overpotential on Ti foil, as shown in Fig. 1b, c, respectively. When the concentration is very low (≤0.001%), slight APMs are adsorbed onto the metal substrate (Fig. 1a(1)), and the electrochemical behavior of the Zn metal anode remains mostly the same as in the electrolyte without additives. At an intermediate concentration (~0.01%), the APMs begin to adsorb onto the substrate in a loosely packed layout (Fig. 1a(2)), and an increase in interface

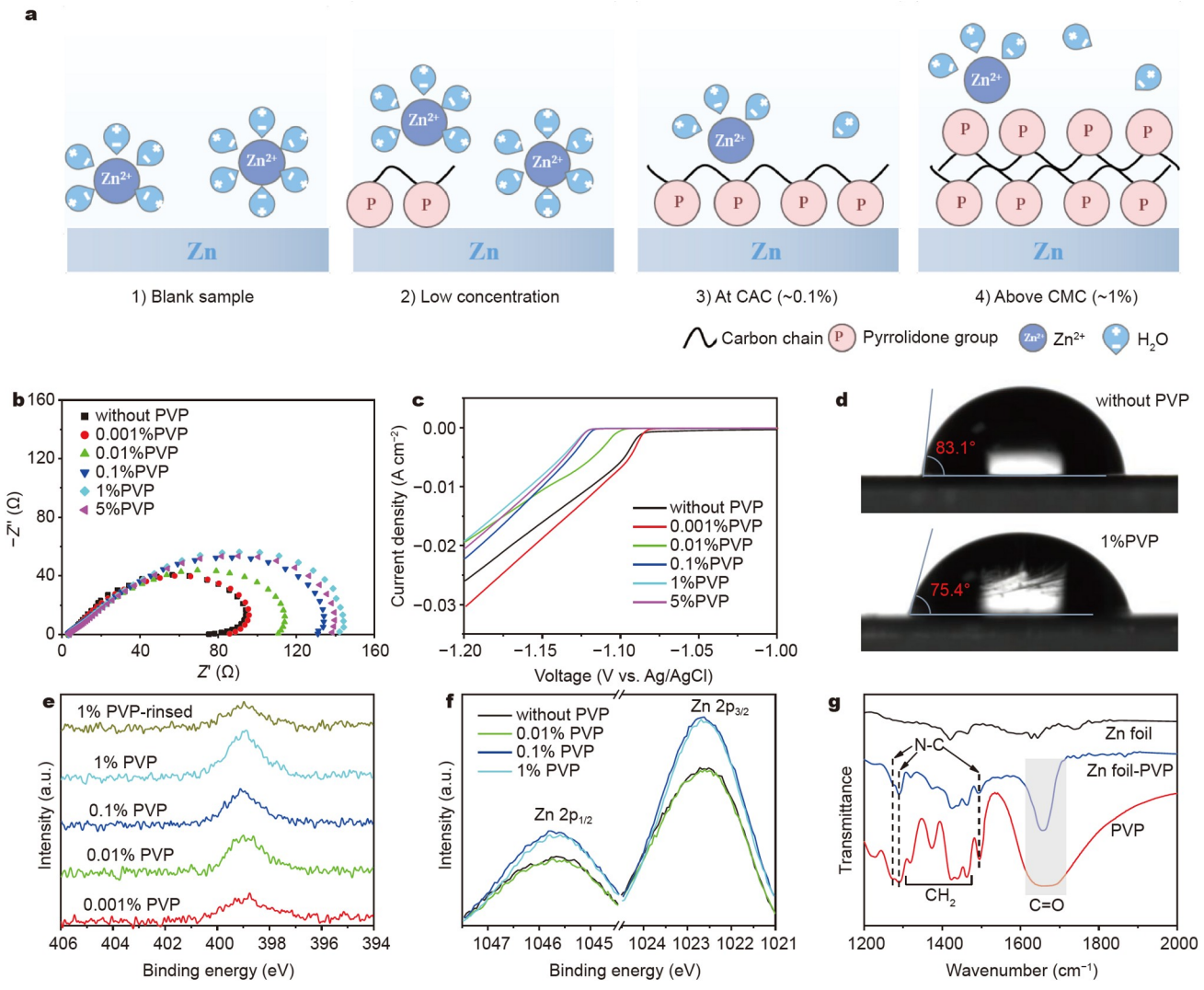

Figure 1 (a) Schematic illustration of the self-assembly processes of AEEI as the concentration of APMs in the electrolyte increases; corresponding (b) EIS Nyquist plots of the Zn metal anode and (c) LSV curves of Ti foil in electrolytes with various concentration of PVP APMs obtained in a three-electrode configuration using Zn metal as the counter electrode and Ag/AgCl as the reference electrode; (d) the contact angle of different electrolyte droplets on the Zn electrode; XPS (e) N 1s spectra of the Zn electrodes and (f) Zn 2p spectra of copper electrodes with AEEI formed in various concentrations of PVP APMs; (g) ATR-FTIR spectra of pure PVP and Zn electrodes of pristine and with AEEI.

impedance, as well as nucleation overpotential, is observed, caused by the block effect of adsorbed APMs. When the concentration increases to the CAC (~0.1%), a relatively uniform layer of APMs (i.e., AEEI) assembles on the substrate (Fig. 1a(3)) and an additional rise in interface impedance, together with nucleation overpotential, can be recorded. With further increase of concentration up to and beyond the critical micelle concentration (CMC, ~1%), a uniform and compact lamellar micelle of APMs finally assembles at the substrate-electrolyte interface to form a dense AEEI (Fig. 1a(4)). At this time, the interface impedance and nucleation overpotential remain relatively steady with little increase, because of a stable micellar interphase. It should be noted that the interface impedance with 5% PVP appears comparable to that of 1%. The little reduction in impedance observed with the 5% sample may be linked to the high sensitivity of EIS due to small variations in the area of the electrode or geometric symmetry [47,48]. In addition, contact angles between electrolyte and Zn metal show a decline trend from 83.1° to 73.4° as the concentration of PVP APMs increases from 0 to 1% (Fig. 1d and Fig. S1), caused by an integrated reduction in surface (electrolyte-vapor) and interface (metal-electrolyte) tension. This further suggests that APMs in the electrolyte favors distribution at the Zn metal-electrolyte interface and improves the wettability of the electrode, which decreases interfacial free energy for conformal Zn deposition [49].

To prepare electrodes with AEEI on the surface for analysis, electrodes were soaked in electrolytes with various concentrations of APMs to assemble AEEI on their surfaces. Subsequently, they were spin-dried to eliminate any interference from possible residual liquid electrolyte. Zn metal electrodes with AEEI formed in various concentrations were investigated using XPS, and characteristic N species in PVP were used as the indicators of AEEI. It can be seen from the XPS N 1s spectra (Fig. 1e) that all samples show a peak centered at 398.9 eV. The peak intensity, namely PVP content in AEEI, firstly increases as the concentration stays at the low region (0–0.1%), and then becomes steady when the concentration is further increased up to CMC (~1%). These results match well with the evolution of electrochemical behaviors of the Zn metal anode in electrolytes with different concentrations of PVP APMs as mentioned above, confirming the successful formation of AEEI at CMC. It should be noted that no shift or additional peak is observed for the N 1s spectra for various electrodes compared to that of pure PVP (Fig. S2a), indicating that N atoms in the PVP molecules do not participate in the interaction with zinc. To clarify the distribution of Zn^{2+} ions at the electrode-electrolyte interface, XPS Zn 2p spectra (Fig. 1f) were also conducted on copper electrode with AEEI to eliminate interference from the intense Zn^0 signal of the Zn metal. All of the electrodes exhibit two peaks around 1022.6 and 1045.7 eV, corresponding to the $2p_{3/2}$ and $2p_{1/2}$ states of Zn^{2+} ions, respectively. It can be inferred from the peak intensity that the adsorbed Zn^{2+} ions on the electrode retain a similarly low amount when there is no or low concentration (0.01%) of APMs in the electrolyte as few AEEI is formed. Meanwhile, the amount of adsorbed Zn^{2+} ions increases and then remains at the same high level as the concentration increases up to and beyond the CAC (~0.1%) after the formation of AEEI. These results demonstrate that the AEEI favors the adsorption of Zn^{2+} ions. This is due to the fact that carbonyl oxygen atoms in PVP molecules have a high electron-donating property because of their conjugation with aromatic pyrrole rings. Thus, the oxygen atoms in PVP have an enhanced coordinate attraction with Zn^{2+} ions, as compared to the oxygen atoms in H_2O with lone electron pairs [50,51]. This interaction can be verified from the broadening of the Zn 2p peaks towards lower binding energies, comparing the electrodes with well-formed AEEI (at PVP concentrations $\geqslant$ 0.1%) to those with few AEEI, which can be explained by charge transfer from the carbonyl oxygen of PVP molecules in AEEI to Zn^{2+} ions [52,53]. In addition, the electron-donating state of carbonyl oxygen is consistent with the binding energy upward shift (as compared with pure PVP) of the O1s peak of the electrodes with well-formed AEEI (at PVP concentrations $\geqslant$ 0.1%) (Fig. S2b). Although, a comprehensive resolution of the O1s spectra is troublesome due to the existence of various O species, the coordination interaction between PVP and Zn^{2+} ions at the electrode-electrolyte interface would be beneficial for the desolvation processes of hydrated Zn^{2+} ions, facilitating adequate charge transfer at the interface [50,54].

To explore the interaction between the Zn electrode and PVP molecules in the AEEI, ATR-FTIR spectra of pure PVP and Zn electrodes of pristine and AEEI (formed in 1% PVP electrolyte without $Zn(OTf)_2$ to eliminate interference from Zn^{2+} ions), were recorded, as displayed in Fig. 1g. For pure PVP, characteristic bands can be detected: An intense band at 1667 cm^{-1} from the stretching vibration of C=O, multiple bands between 1300 and 1480 cm^{-1} arisen from typical C–H vibrations in PVP, two bands around 1280 cm^{-1} and an absorption at 1495 cm^{-1} corresponding to the stretching vibrations of N–C bonds from the two distinct N–C–R groups and the N–C=O group, respectively [53,55]. The spectrum of pristine Zn electrode only showes two weak bands around 1400–1480 and 1615–1780 cm^{-1}, which can be assigned to small quantities of organic contaminant and the deformation vibrations of O–H from some surface –OH groups or adsorbed H_2O, respectively. Typical absorption bands from PVP molecules can also be seen in the spectrum of the Zn electrode with AEEI. Particularly, a significant red shift of the C=O stretching vibration from 1667 cm^{-1} for pure PVP to 1658 cm^{-1} is observed. This result clearly suggests that PVP molecules in the AEEI absorb onto the Zn metal through the carbonyl oxygen atoms, leading to weakening of the C=O bond [53]. While no shift is detected for the vibration bands of C–H and N–C, this is consistent with the XPS N 1s result in which N does not interact with zinc. The restricted interaction between N atoms and zinc can be attributed to spatial hindrance, arising from the bonding of an N atom with three adjacent carbon atoms. Additionally, the conjugation of the lone pair electrons, in the unhybridized p orbital of the sp^2 hybridized N atoms, with the pyrrolidone ring makes it challenging for these electrons to readily engage with the surrounding environment, contrasting with the more accessible unshared lone electron pairs in carbonyl oxygen atoms. Moreover, the AEEI can be washed away to some extent, as indicated by the decline in XPS N 1s signals of the sample soaked in 1% PVP electrolyte following a rinsing process (Fig. 1e). It implies that the interaction between carbonyl oxygen and Zn metal is relatively weak, and that desorption of the PVP molecules within the AEEI would occur if the concentration of PVP falls below CAC. In this case, the AEEI would disintegrate if PVP is consumed in some ways. However, as long as the concentration of PVP is reserved above CAC in the electrolyte, the AEEI will spontaneously self-assemble at the electrode-electrolyte interface

with an intrinsic stability. Based on the preceding analysis and discussion, it is evident that the amphiphilic nature of PVP APMs facilitates its assembly of a stable micellar layer at the Zn electrode-electrolyte interface, thereby constructing the framework of AEEI. The carbonyl oxygen atoms of PVP molecules within the framework not only interact with Zn metal electrode, but also coordinate with Zn^{2+} ions, essentially ensuring a stable AEEI with rich Zn^{2+} ions formed on the Zn surface. Such an AEEI, functioning as a form of SEI, is expected to bring a multitude of benefits in enabling a highly reversible Zn metal anode.

Galvanostatic charge-discharge behavior of symmetrical Zn cells with 40 μL electrolyte of various concentrations of APMs in coin-type cells is compared in Fig. 2a. The overpotentials of the cells remain almost unchanged at low concentrations (≤0.01%) below the CAC, except for a voltage fluctuation coming from the 0.01% PVP sample, probably due to nonuniform adsorption of PVP molecules. When the PVP concentration increases to the CAC (~0.1%), a uniform AEEI is formed, resulting in a substantial increase in cell overpotentials, from ~20 mV to more than 110 mV, due to the spatial block effect of the AEEI. No obvious increase of overpotentials is detected when further increasing concentration to the CMC (~1%), showing that the block effect of AEEI remains relatively steady beyond CAC [40]. It should be noted that a moderate rise in interface impedance is observed in Fig. 1b when increasing the PVP concentration from 0 to 0.01%, contrasting to the unchanged overpotentials in the symmetrical Zn cell. This difference can be ascribed to the fact that PVP would adsorb onto the component surfaces of the coin-type cell, leading to a decrease in PVP concentration of the finite volume (40 μL) of electrolyte. When the quantity of electrolyte is adequate (4000 μL) in an electrolytic tank cell, a rise in overpotential to ~100 mV of the 0.01% PVP electrolyte is recorded, as displayed in Fig. S3a. The adsorption of PVP on component surfaces cannot affect the concentration much, when it is in consideration to a large quantity of electrolyte. Meanwhile, no change in overpotential is observed at PVP concentration of 0.001% at small or large quantities of electrolyte, as showed in Fig. S3b. These results verify that ~0.01% is the critical concentration at which PVP molecules begin to assemble on Zn electrode and generate a block effect, and that few PVP molecules could be distributed at the interface below this concentration. This once again emphasizes the importance of PVP concentration in forming the AEEI. It should be clarified that zinc deposition is confined to the bottom side of the AEEI, specifically on the side facing the zinc electrode, considering the rather poor electrical conductivity of the AEEI. Zinc ions need to traverse the AEEI layer before depositing on the surface of the zinc metal, which explains the increased interfacial impedance after the formation of AEEI. In addition, because of their analogous APM structure with hydrophilic pyrrolidone groups like PVP, APMs of 1-Octyl-2-pyrrolidinone can also form effective AEEI on the Zn anode, as can be inferred from the similar trend in overpotential when increasing their concentrations in electrolytes (Fig. S4). This implies that the construction of AEEI using APMs is applicable for generalization.

The block effect of AEEI can protect Zn metal from the active H_2O and suppress side reactions. LSV was conducted to investigate the influence of PVP concentration on HER with a three-electrode configuration in 2 M LiOTf aqueous electrolyte (to avoid interference from Zn deposition) using Ag/AgCl as the reference electrode, and Pt foil as the working and counter electrodes. As shown in Fig. 2b, the HER current in 1% PVP electrolyte with a dense AEEI is remarkably reduced compared

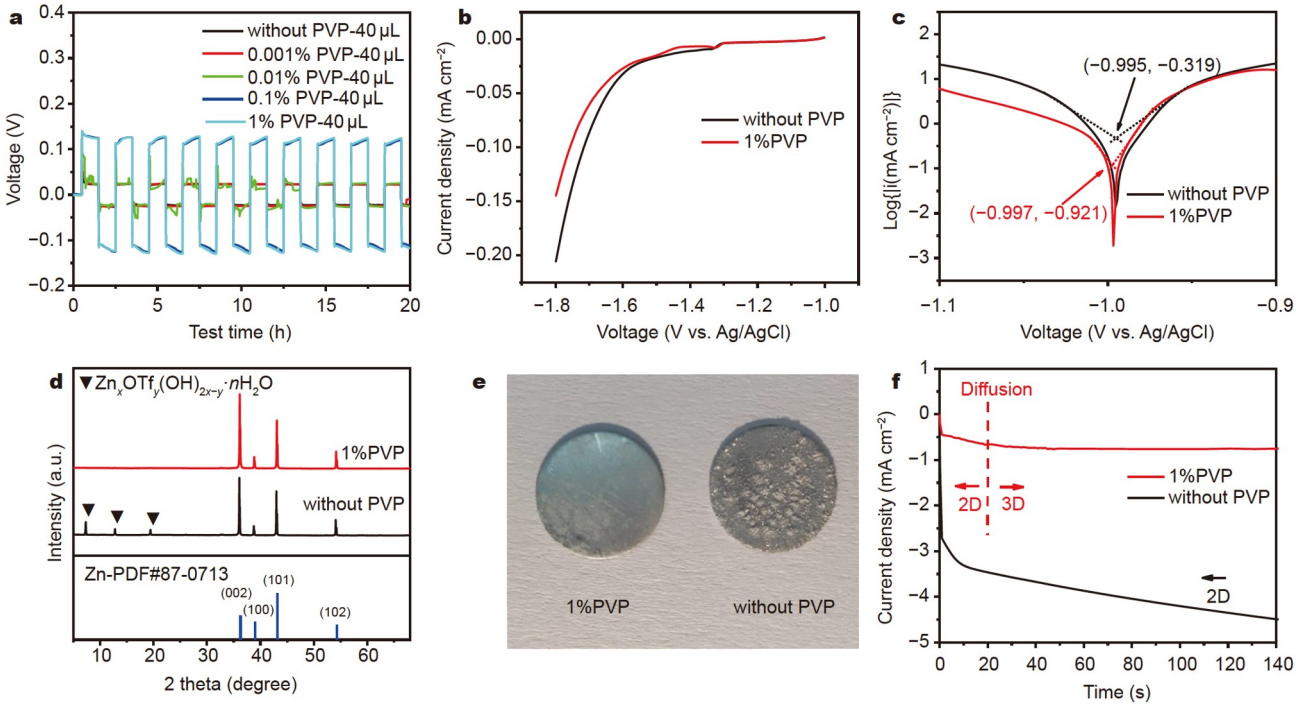

Figure 2 (a) Voltage-time curves of symmetric Zn cells in electrolytes of various concentrations of APMs at 1.0 mA cm^{-2} and 1 mA h cm^{-2}; (b) LSV curves of the Pt foil electrode in 2 M LiOTf aqueous electrolyte; (c) linear polarization curves of the Zn metal electrode in the $Zn(OTf)_2$ electrolyte with 0 and 1% PVP; (d) XRD pattern of Zn metal electrodes after 60 cycles at 1 mA cm^{-2} and 1 mA h cm^{-2}; (e) optical photos of Zn electrodes after being immersed in different electrolytes for 7 days at 30°C; (f) chronoamperograms of the Zn electrode at an overpotential of −200 mV in different electrolytes.

to the case without PVP. The suppression of side reactions is further confirmed by the Zn metal corrosion current and potential as demonstrated by the Tafel plots in Fig. 2c. The fitted results reveal a substantial decline of corrosion current from 0.48 to 0.12 mA cm^{-2} coupled with a slight decrease in corrosion potential from −995 to −997 mV when increasing the PVP concentrations from 0 to 1%. Moreover, possible by-products of the cycled Zn metal electrodes (60 cycles at 1.0 mA cm^{-2} and 1.0 mA h cm^{-2}) in 0 and 1% PVP electrolyte were characterized using XRD (Fig. 2d). The XRD of Zn metal electrode cycled in 1% PVP electrolyte shows characteristic peaks of hexagonal Zn metal (PDF#87-0713) without any other peaks. However, additional peaks at 6.6°, 13.2°, and 19.8° corresponding to byproducts of $Zn_xOTf_y(OH)_{2x-y}{\cdot}nH_2O$ induced by severe local HER reaction [56] can be detected in the XRD pattern of the electrode cycled in the electrolyte without PVP. This further proves that side reactions can be drastically suppressed by the AEEI. To demonstrate the protective capability of PVP additive under non-operating conditions, Zn foil was immersed in 0 and 1% PVP electrolyte for 7 days, respectively. As shown in Fig. 2e, the Zn foil after soaking in 0% PVP electrolyte suffers from severe corrosion, displaying a coarse and porous surface with obvious indictors of many by-products. On the other hand, the Zn foil soaked in 1% PVP electrolyte is barely corroded, displaying a smooth surface, suggesting that PVP can effectively prevent the corrosion of Zn metal under non-operating conditions.

The nucleation and growth processes of Zn deposition in electrolytes with and without 1% PVP were studied *via* chronoamperometry by applying a potential of 200 mV to the Zn electrode to obtain the current-time curves, as exhibited in Fig. 2f. It is found that the current density of the Zn electrode in electrolyte without PVP increases continuously after 20 s, indicating a prolonged and uncontrolled 2D diffusion process [57]. In this case, the absorbed Zn^{2+} ions tend to diffuse laterally along the electrode surface, aggregate and grow into dendrites to minimize the surface energy (specifically, interfacial energy in the electrolyte). In comparison, Zn electrode in 1% PVP electrolyte exhibits a stable and lower current density after a shorter 2D diffusion (within 20 s), suggesting that adsorbed Zn^{2+} ions appear to be reduced to metallic Zn locally with a constant 3D diffusion process [58]. This improvement can be ascribed to two reasons. Firstly, the reduced interfacial energy from the formation of AEEI on Zn electrode decreases the 2D diffusion driving force. Secondly, the coordination interaction between the carbonyl oxygen atoms of PVP molecules in the AEEI and Zn^{2+} ions magnifies the energy barrier for absorbed Zn^{2+} ions to move laterally, thereby facilitating the local reduction of Zn^{2+} ions and conformal Zn deposition.

Zn deposition morphology

Scanning electron microscopy (SEM) and *in situ* optical microscopy were employed to investigate the morphology of Zn deposition [59]. Fig. 3a, b show SEM images of Zn deposition on Zn electrodes at 1 mA cm^{-2} and 2 mA h cm^{-2} in 1 M $Zn(OTf)_2$ aqueous electrolyte with 0 and 1% PVP. Heterogeneous and porous Zn deposition is observed across the wide range of the electrode in the electrolyte without PVP (Fig. 3a). The magnified image in the inset reveals a vertically arrayed plate-like Zn morphology. In sharp contrast, the Zn deposition is conformal and compact without any cracks or pores in the electrolyte with 1% PVP, as can be seen in Fig. 3b. In comparison with the SEM images obtained before zinc deposition (Fig. S5), it is evident that the morphology of the zinc deposits in the 1% PVP electrolyte exhibits minimal discernible changes with a rather flat surface. Conversely, in the absence of PVP in the electrolyte, significant alterations with rugged morphology are observed after zinc deposition. This indicates that the AEEI ensures a conformal Zn deposition morphology, a benefit of its ability to suppress water decomposition side reactions and restrict unfavorable 2D diffusion. AEEI is thus expected to guide dendrite-free Zn deposition. Fig. 3c, d show the energy dispersive X-ray spectroscopy (EDS) mapping of N and C, respectively, for the Zn deposited electrode in the electrolyte with 1% PVP. Distinct N and C signals can be seen uniformly distributed across the Zn electrode, indicating that some adsorbed PVP molecules are possibly co-deposited into the Zn electrode [60]. This would lead

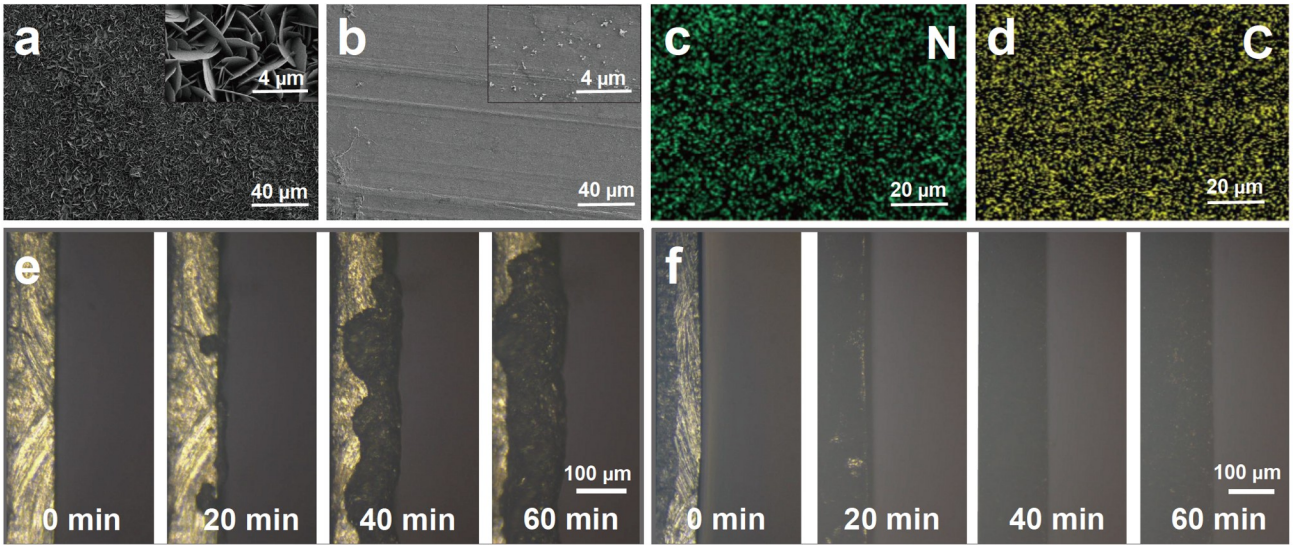

Figure 3 SEM images of the Zn anode after deposition at 1 mA cm^{-2} and 2 mA h cm^{-2} in electrolyte with (a) 0 and (b) 1% PVP; EDS mapping of (c) N and (d) C elements of the Zn anode after deposition in the electrolyte with 1% PVP; *in situ* optical microscope images of the Zn plating process in the electrolyte with (e) 0 and (f) 1% PVP at 10 mA cm^{-2}.

to the consumption of PVP and a reserve of PVP beyond the AEEI formation concentration (CAC, ~0.1%) in the electrolyte, essential to maintaining a stable AEEI.

To investigate the dendrite growth phenomenon, an *in situ* optical microscope was employed to view the Zn plating process in electrolytes with 0 or 1% PVP at a high current of 10 mA cm^{-2} for 60 min [61]. In the electrolyte with 0% PVP, as the deposition time increases, uneven Zn plating with dendritic growth appears on the surface and side of the zinc foil (Fig. 3e). The heterogeneity of the Zn deposition layer gradually amplifies as the plating process progresses. In this case, critical Zn dendrites that could penetrate through the separator eventually form, leading to the failure of the cell. In the electrolyte with 1% PVP (Fig. 3f), however, Zn plating is smooth and homogeneous, and no apparent Zn dendrites are found even after 60 min (10 mA h) of plating. The results demonstrate that AEEI promotes dendrite-free Zn deposition. The electrode-scale homogeneous Zn deposition in PVP electrolyte can contribute to excellent cycling stability of Zn anode under high current.

Electrochemical performance

The cycling stability of Zn anodes in electrolytes with various PVP concentrations were investigated using coin-type Zn||Zn symmetrical cells, as show in Fig. 4a. A small overpotential of 20 mV was observed during Zn deposition and dissolution in electrolyte without PVP at 1 mA cm^{-2} and 1 mA h cm^{-2}. It suggested intrinsic fast kinetics of Zn deposition-dissolution reactions at the interface, which was reported to facilitate Zn dendrites growth at a nonuniform Zn anode-electrolyte interface [62]. The cell with 0% PVP electrolyte was short circuited after

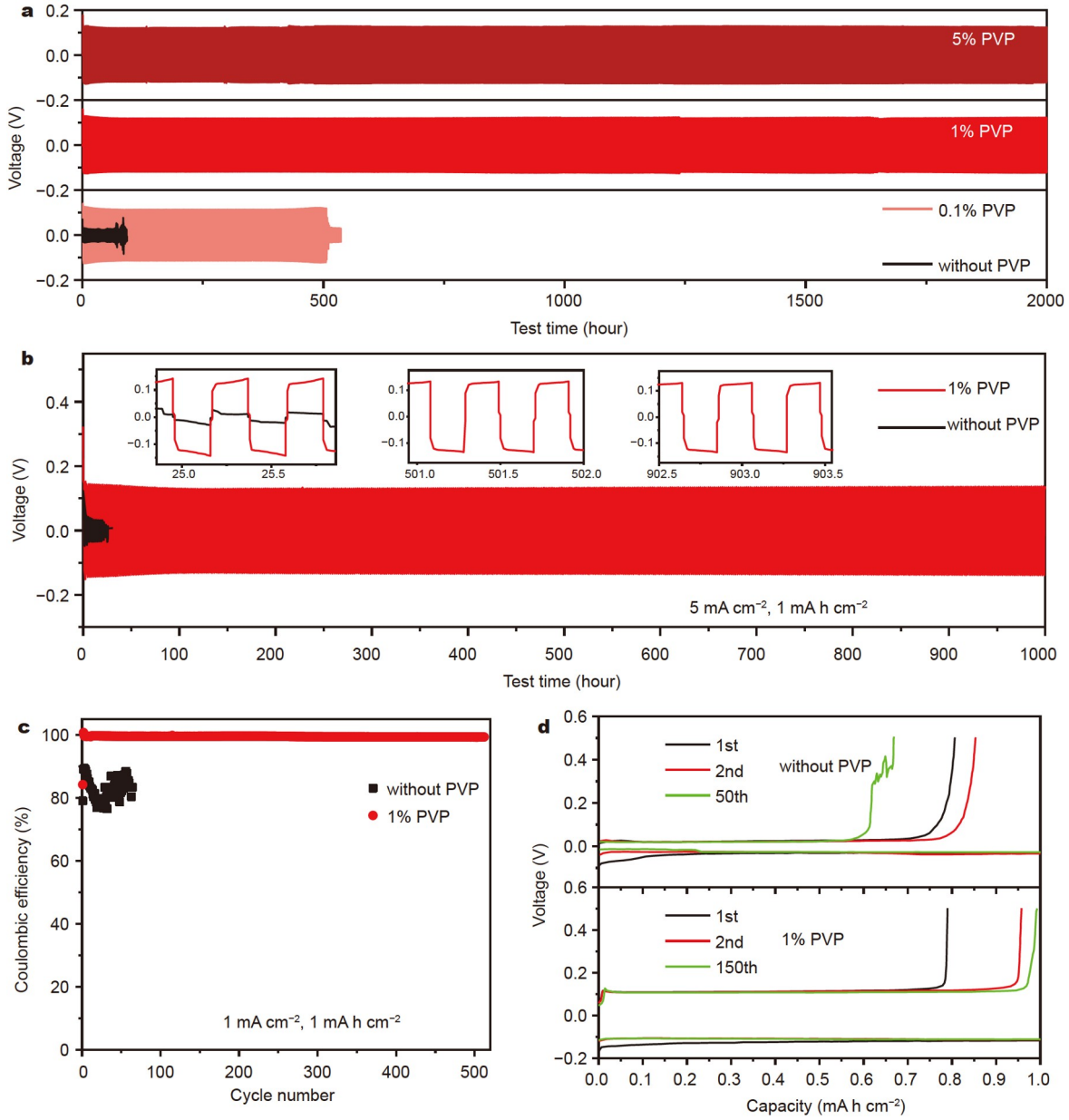

Figure 4 Long-term cycle performance of Zn||Zn symmetrical cells with different electrolytes at (a) 1 mA cm^{-2} and 1 mA h cm^{-2} and (b) 5 mA cm^{-2} and 1 mA h cm^{-2}; (c) the cycle CE of Zn||Ti cells in different electrolytes; (d) the corresponding charge-discharge curves of different cycles at 1 mA cm^{-2} and 1 mA h cm^{-2}.

only 100 h due to severe Zn dendrites. When 0.1% or more PVP was added in the electrolyte, an AEEI was formed and, therefore, the overpotential was increased to ~120 mV. The cycle life of the cell with 0.1% PVP electrolyte was increased to 500 h before a final short circuit. Further increase of PVP concentration to 1% and 5% enabled a cycle life of more than 2000 h of the cell. At an even higher concentration of 10%, the cycle life of the symmetrical cell still maintained the same level as 1% and 5% (Fig. S6), manifesting that AEEI preserved a similar protective effect over long-term cycles above a concentration of 1%. The relatively short cycle life of the 0.1% PVP electrolyte could be ascribed to the fact that PVP is consumed during cycling as mentioned above and the concentration is decreased to blow the CAC where a stable AEEI can be formed. At concentrations above 1%, adequate PVP is reserved in the electrolyte to maintain the concentration above CAC despite some consumption. Stable AEEI was maintained over the entire cycling to suppress side reactions and guide conformal Zn deposition, which guaranteed a long cycle life of the Zn metal anode. The stability of AEEI can be verified from the little increased interfacial impedance of the Zn||Zn symmetrical cell using electrolyte with 1% PVP over 100 cycles (Fig. S7). Moreover, XPS survey and N 1s spectra (Fig. S8) of the Zn electrodes cycled in symmetrical cells with 1%PVP are nearly the same at the 5th and 100th cycle, further demonstrating the stability of AEEI. Since the effectiveness of PVP saturates beyond the concentration of 1%, electrolyte with 1% PVP is identified as optimized, considering the cost and potential impacts on the aqueous electrolyte system. The AEEI works well under high current density. The electrolyte with 1% PVP dramatically improves the cycle life of Zn anode at 2 mA cm^{-2} (Fig. S9) and 5 mA cm^{-2} (Fig. 4b) from tens of hours to more than 1000 h. Moreover, a Zn||Zn symmetrical cell using electrolyte with 1% PVP maintaines a cycle life of over 800 h at 2 mA cm^{-2} and 2 mA h cm^{-2} and can work over 250 h even at 5 mA cm^{-2} and 5 mA h cm^{-2} (Fig. S10), showing the merit of AEEI at harsh condition of high capacity.

The cycle CE of Zn anodes in aqueous electrolytes with different PVP concentrations was investigated using coin-type Zn||Ti cells, as displayed in Fig. 4c, d. At 1 mA cm^{-2} and 1 mA h cm^{-2}, the cell with 0% PVP electrolyte showed a maximum CE of 89.4% in the third cycle, which quickly decreased and fluctuated around 85% after initial cycles, and failed only after ~60 cycles. The low CE suggests continuous interfacial side reactions of the Zn metal anode in this electrolyte. In contrast, the CE of the cell in electrolyte with 1% PVP quickly reached 99.7% after the initial two cycles and retained at more than 99.2% over 500 cycles (i.e., 1000 h). This result indicates that side reactions such as HER can be drastically suppressed by the block effect of AEEI. Furthermore, an increased voltage hysteresis was noted in the cell utilizing the 1% PVP electrolyte as shown in Fig. 4d. This phenomenon can be ascribed to the existence of AEEI, leading to additional interfacial impedance and heightened polarization.

Full cell performance

Finally, full cells based on Zn anode and V_2O_5 cathode were fabricated to verify the feasibility of the PVP-based AEEI. The V_2O_5 cathode was prepared from commercial V_2O_5 powder. The reported specific capacity and applied current density were calculated on the basis of the mass of V_2O_5 [63]. Fig. 5a compares the rate capability of the Zn||V_2O_5 cells with electrolyte of 0 and 1% PVP. The capacities in 1 M $Zn(OTf)_2$ with 1% PVP are 226, 211, 194, 163, and 117 mA h g^{-1} at current densities of 2, 5, 10, 20, and 40 A g^{-1}, respectively, which are slightly higher than those in the 1 M $Zn(OTf)_2$ system. The higher capacity may be explained by the better cycling stability of the cells in electrolyte with PVP. Fig. S11 displays the long-term cycle performance of the Zn||V_2O_5 cells using electrolytes with 0 and 1% PVP at 2 A g^{-1}. The cell with 1% PVP electrolyte works well over 1500 cycles, in contrast to a short circuit after ~900 cycles of the cell with 0% PVP electrolyte. Moreover, capacity retention of 76% is achieved in the 1% PVP electrolyte after 500 cycles, outperforming that of 42% in the electrolyte without PVP.

To further evaluate the advantages of high CE offered by the AEEI, a thin Zn-metal foil of 30 μm thickness was used to assemble the Zn||V_2O_5 full cells. The typical discharge/charge profiles in different cycles of these Zn||V_2O_5 cells with 0 or 1% PVP electrolyte at 2 A g^{-1} are shown in Fig. 5b. The cells with different electrolytes exhibit similar charge-discharge profiles, indicating that the PVP additive does not affect the cathode much. The long-term cycling performance of these cells is illustrated in Fig. 5c. A remarkable capacity of 182 mA h g^{-1} with a capacity retention of 80% is achieved in the electrolyte with 1% PVP after 200 cycles, significantly outperforming that in electrolyte without PVP (60 mA h g^{-1} with 30% retention). Notably, the 1 M $Zn(OTf)_2$ with 1% PVP electrolyte enables an ~100% CE during battery operation, while a continuous fluctuation of CE is observed in the electrolyte without PVP, as caused by the interfacial side reactions (e.g., H_2 evolution and Zn corrosion). Thus, the PVP additive efficiently improves the cycling of the Zn||V_2O_5 battery by mitigating the degradation of the Zn anode, benefitting from a stable AEEI.

CONCLUSIONS

In summary, a novel electrode-electrolyte interphase self-assembled from the electrolyte additive of APMs in 1 M Zn $(OTf)_2$ aqueous electrolyte has been presented. PVP is selected as a demonstrating type of APMs due to the high electron-donating property of their carbonyl oxygen atoms that conjugate with aromatic pyrrole rings. PVP APMs are driven to assemble and distribute on the hydrophilic Zn metal surface because of their APM structures. The concentration of APMs is the crucial factor that affects the self-assemble process. A lamellar micelle of APMs with rich Zn^{2+} ions will eventually be constructed on the electrode surface, forming a stable AEEI if the concentration of APMs reaches and exceeds the CAC (~0.1%). In addition, it is found that the structure and stability of this AEEI are essentially guaranteed by the carbonyl oxygen atoms of PVP molecules, which not only interact with the Zn metal electrode, but also coordinate with Zn^{2+} ions, as revealed by the XPS and FTIR results. The as-formed AEEI can block Zn metal from direct contacting with active H_2O and effectively suppress side reactions. Moreover, the AEEI exhibits a strong propensity to restrict unfavorable 2D diffusion of Zn^{2+} ions because of a decreased 2D diffusion driving force and magnified energy barrier for lateral movement, which can be attributed to the reduced interfacial energy through AEEI formation and the coordination between the carbonyl oxygen and Zn^{2+} ions, respectively. Accordingly, conformal and dendrite-free Zn deposition is achieved with the assistance of this AEEI. Importantly, the AEEI is spontaneously self-assembled and distributed at the electrode-electrolyte interface. It intrinsically possesses a high stability and avoids the

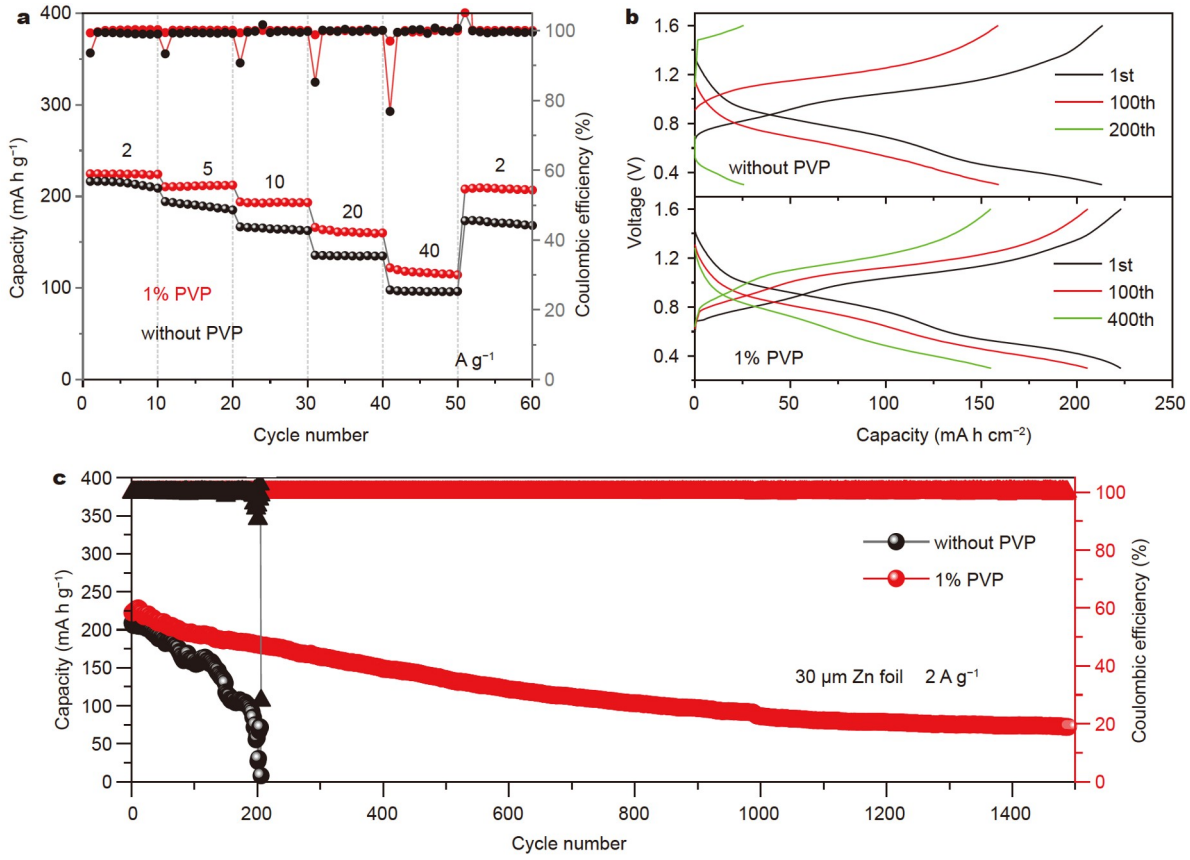

Figure 5 (a) Rate capability of Zn||V_2O_5 cells using different electrolytes; (b) typical charge-discharge curves and (c) cycle performance of the Zn||V_2O_5 full cells at 2 A g^{-1} with the Zn metal anode of 30-μm thickness.

risk of cracks and peeling off, as long as the concentration of PVP is reserved above CAC in the electrolyte. As a consequence, a long cycle life of over 2000 h of the Zn||Zn symmetric cell at 1 mA cm^{-2} and 1 mA h cm^{-2} and CE above 99.2% over 500 cycle of the Zn||Ti cell are achieved in 1 M $Zn(OTf)_2$ electrolyte with 1% PVP. In a V_2O_5||Zn full cell, the V_2O_5 cathode delivers an initial capacity of 226 mA h g^{-1} and maintains capacity retention of 76% after 500 cycles in the 1% PVP electrolyte, which is much higher than the value of 42% in the electrolyte without PVP.

Received 22 December 2023; accepted 1 April 2024; published online 11 June 2024

1 Fang G, Zhou J, Pan A, *et al.* Recent advances in aqueous zinc-ion batteries. ACS Energy Lett, 2018, 3: 2480–2501
2 Song J, Xu K, Liu N, *et al.* Crossroads in the renaissance of rechargeable aqueous zinc batteries. Mater Today, 2021, 45: 191–212
3 Wang R, Yao M, Huang S, *et al.* An anti-freezing and anti-drying multifunctional gel electrolyte for flexible aqueous zinc-ion batteries. Sci China Mater, 2022, 65: 2189–2196
4 Lin C, Liu Y, Zhang X, *et al.* Regulating the plating process of zinc with highly efficient additive for long-life zinc anode. J Power Sources, 2022, 549: 232078
5 Chen W, Li G, Pei A, *et al.* A manganese-hydrogen battery with potential for grid-scale energy storage. Nat Energy, 2018, 3: 428–435
6 Liang Y, Dong H, Aurbach D, *et al.* Current status and future directions of multivalent metal-ion batteries. Nat Energy, 2020, 5: 646–656
7 Geng Y, Pan L, Peng Z, *et al.* Electrolyte additive engineering for aqueous Zn ion batteries. Energy Storage Mater, 2022, 51: 733–755
8 Shen Q, Wang Y, Han G, *et al.* Recent progress in electrolyte additives for highly reversible zinc anodes in aqueous zinc batteries. Batteries, 2023, 9: 284
9 Li D, Cao L, Deng T, *et al.* Design of a solid electrolyte interphase for aqueous Zn batteries. Angew Chem Int Ed, 2021, 60: 13035–13041
10 Chen W, Guo S, Qin L, *et al.* Hydrogen bond-functionalized massive solvation modules stabilizing bilateral interfaces. Adv Funct Mater, 2022, 32: 2112609
11 He W, Zuo S, Xu X, *et al.* Challenges and strategies of zinc anode for aqueous zinc-ion batteries. Mater Chem Front, 2021, 5: 2201–2217
12 Zheng X, Ahmad T, Chen W. Challenges and strategies on Zn electrodeposition for stable Zn-ion batteries. Energy Storage Mater, 2021, 39: 365–394
13 Wang S, Wang Z, Yin Y, *et al.* A highly reversible zinc deposition for flow batteries regulated by critical concentration induced nucleation. Energy Environ Sci, 2021, 14: 4077–4084
14 Yang X, Li C, Sun Z, *et al.* Interfacial manipulation *via in situ* grown ZnSe cultivator toward highly reversible Zn metal anodes. Adv Mater, 2021, 33: e2105951
15 Zhou T, Shen J, Wang Z, *et al.* Regulating lithium nucleation and deposition *via* MOF-derived Co@C-modified carbon cloth for stable Li metal anode. Adv Funct Mater, 2020, 30: 1909159
16 Zeng L, Zhou T, Xu X, *et al.* General construction of lithiophilic 3D skeleton for dendrite-free lithium metal anode *via* a versatile MOF-derived route. Sci China Mater, 2022, 65: 337–348
17 Wang L, Zhou S, Yang K, *et al.* Screening selection of hydrogen evolution-inhibiting and zincphilic alloy anode for aqueous Zn battery. Adv Sci, 2024, 11: 2307667
18 Chen S, Li S, Ma L, *et al.* Asymmetric anion zinc salt derived solid electrolyte interphase enabled long-lifespan aqueous zinc bromine batteries. Angew Chem Int Ed, 2024, 63: e202319125
19 Liu C, Xu W, Zhang L, *et al.* Electrochemical hydrophobic Tri-layer

interface rendered mechanically graded solid electrolyte interface for stable zinc metal anode. Angew Chem Int Ed, 2024, 63: e202318063
20 Zhang W, Zhu X, Kang L, *et al.* Stabilizing zinc anode using zeolite imidazole framework functionalized separator for durable aqueous zinc-ion batteries. J Energy Chem, 2024, 90: 23–31
21 Yan H, Li S, Zhong J, *et al.* An electrochemical perspective of aqueous zinc metal anode. Nano-Micro Lett, 2023, 16: 15
22 Kang L, Cui M, Jiang F, *et al.* Nanoporous $CaCO_3$ coatings enabled uniform Zn stripping/plating for long-life zinc rechargeable aqueous batteries. Adv Energy Mater, 2018, 8: 1801090
23 Wang L, Zhang L, Meng Y, *et al.* Fluorinated hybrid interphases enable anti-corrosion and uniform zinc deposition for aqueous zinc metal batteries. Sci China Mater, 2023, 66: 4595–4604
24 Zhao Z, Zhao J, Hu Z, *et al.* Long-life and deeply rechargeable aqueous Zn anodes enabled by a multifunctional brightener-inspired interphase. Energy Environ Sci, 2019, 12: 1938–1949
25 Chen D, Wang H, Ren L, *et al.* Zinc-ion conductive buffer polymer layer eliminating parasitic reactions of Zn anode in aqueous zinc-ion batteries. Sci China Mater, 2023, 66: 4605–4614
26 Wang Z, Chen H, Wang H, *et al. In Situ* growth of a metal-organic framework-based solid electrolyte interphase for highly reversible Zn anodes. ACS Energy Lett, 2022, 7: 4168–4176
27 Cao L, Li D, Deng T, *et al.* Hydrophobic organic-electrolyte-protected zinc anodes for aqueous zinc batteries. Angew Chem Int Ed, 2020, 59: 19292–19296
28 He W, Gu T, Xu X, *et al.* Uniform *in situ* grown ZIF-L layer for suppressing hydrogen evolution and homogenizing Zn deposition in aqueous Zn-Ion batteries. ACS Appl Mater Interfaces, 2022, 14: 40031–40042
29 Zeng X, Mao J, Hao J, *et al.* Electrolyte design for *in situ* construction of highly Zn^{2+}-conductive solid electrolyte interphase to enable high-performance aqueous Zn-Ion batteries under practical conditions. Adv Mater, 2021, 33: e2007416
30 Guo S, Qin L, Zhang T, *et al.* Fundamentals and perspectives of electrolyte additives for aqueous zinc-ion batteries. Energy Storage Mater, 2021, 34: 545–562
31 Yan D, Yang HY, Bai Y. Tactics to optimize conversion-type metal fluoride/sulfide/oxide cathodes toward advanced lithium metal batteries. Nano Res, 2023, 16: 8173–8190
32 Wang F, Borodin O, Gao T, *et al.* Highly reversible zinc metal anode for aqueous batteries. Nat Mater, 2018, 17: 543–549
33 Qiu H, Du X, Zhao J, *et al.* Zinc anode-compatible *in-situ* solid electrolyte interphase *via* cation solvation modulation. Nat Commun, 2019, 10: 5374
34 Chang N, Li T, Li R, *et al.* An aqueous hybrid electrolyte for low-temperature zinc-based energy storage devices. Energy Environ Sci, 2020, 13: 3527–3535
35 Huang Z, Wang T, Li X, *et al.* Small-dipole-molecule-containing electrolytes for high-voltage aqueous rechargeable batteries. Adv Mater, 2022, 34: e2106180
36 Zhu Y, Hoh HY, Qian S, *et al.* Ultrastable zinc anode enabled by CO_2-induced interface layer. ACS Nano, 2022, 16: 14600–14610
37 Cao L, Li D, Pollard T, *et al.* Fluorinated interphase enables reversible aqueous zinc battery chemistries. Nat Nanotechnol, 2021, 16: 902–910
38 Huang C, Huang F, Zhao X, *et al.* Rational design of sulfonamide-based additive enables stable solid electrolyte interphase for reversible Zn metal anode. Adv Funct Mater, 2022, 33: 2210197
39 Xu X, Su H, Zhang J, *et al.* Sulfamate-derived solid electrolyte interphase for reversible aqueous zinc battery. ACS Energy Lett, 2022, 7: 4459–4468
40 Zhu Y, Free ML, Woollam R, *et al.* A review of surfactants as corrosion inhibitors and associated modeling. Prog Mater Sci, 2017, 90: 159–223
41 Zhang R, Somasundaran P. Advances in adsorption of surfactants and their mixtures at solid/solution interfaces. Adv Colloid Interface Sci, 2006, 123-126: 213–229
42 Cui P, Hu J, Luo Y, *et al.* Trace tea polyphenols enabling reversible dendrite-free zinc anode. J Colloid Interface Sci, 2022, 624: 450–459
43 Zhu Y, Free ML, Yi G. Electrochemical measurement, modeling, and prediction of corrosion inhibition efficiency of ternary mixtures of homologous surfactants in salt solution. Corrosion Sci, 2015, 98: 417–429
44 Möbius D, Miller R, Fainerman VB. Surfactants: Chemistry, interfacial properties, applications. Amsterdam: Elsevier, 2001
45 Fuchs-Godec R, Pavlović MG. Synergistic effect between non-ionic surfactant and halide ions in the forms of inorganic or organic salts for the corrosion inhibition of stainless-steel X_4Cr_{13} in sulphuric acid. Corrosion Sci, 2012, 58: 192–201
46 Guan K, Tao L, Yang R, *et al.* Anti-corrosion for reversible zinc anode *via* a hydrophobic interface in aqueous zinc batteries. Adv Energy Mater, 2022, 12: 2103557
47 Bünzli C, Kaiser H, Novák P. Important aspects for reliable electrochemical impedance spectroscopy measurements of Li-Ion battery electrodes. J Electrochem Soc, 2015, 162: A218–A222
48 Wang S, Zhang J, Gharbi O, *et al.* Electrochemical impedance spectroscopy. Nat Rev Methods Primers, 2021, 1: 41
49 Deng W, Xu Z, Wang X. High-donor electrolyte additive enabling stable aqueous zinc-ion batteries. Energy Storage Mater, 2022, 52: 52–60
50 Chuai M, Yang J, Tan R, *et al.* Theory-driven design of a cationic accelerator for high-performance electrolytic MnO_2-Zn batteries. Adv Mater, 2022, 34: e2203249
51 Ram S, Fecht HJ. Modulating up-energy transfer and violet-blue light emission in gold nanoparticles with surface adsorption of poly(vinyl pyrrolidone) molecules. J Phys Chem C, 2011, 115: 7817–7828
52 Li S, Zhao S, Lu X, *et al.* Low-valence $Zn^{\delta+}$ ($0< \delta <2$) single-atom material as highly efficient electrocatalyst for CO_2 reduction. Angew Chem Int Ed, 2021, 60: 22826–22832
53 Xian J, Hua Q, Jiang Z, *et al.* Size-dependent interaction of the poly(*N*-vinyl-2-pyrrolidone) capping ligand with Pd nanocrystals. Langmuir, 2012, 28: 6736–6741
54 Niu B, Li Z, Luo D, *et al.* Nano-scaled hydrophobic confinement of aqueous electrolyte by a nonionic amphiphilic polymer for long-lasting and wide-temperature Zn-based energy storage. Energy Environ Sci, 2023, 16: 1662–1675
55 García-Aguilar J, Navlani-García M, Berenguer-Murcia Á, *et al.* Evolution of the PVP-Pd surface interaction in nanoparticles through the case study of formic acid decomposition. Langmuir, 2016, 32: 12110–12118
56 Miao L, Wang R, Di S, *et al.* Aqueous electrolytes with hydrophobic organic cosolvents for stabilizing zinc metal anodes. ACS Nano, 2022, 16: 9667–9678
57 Han M, Huang J, Xie X, *et al.* Hydrated eutectic electrolyte with ligand-oriented solvation shell to boost the stability of zinc battery. Adv Funct Mater, 2022, 32: 2110957
58 Zhang H, Guo R, Li S, *et al.* Graphene quantum dots enable dendrite-free zinc ion battery. Nano Energy, 2022, 92: 106752
59 Wang M, Wu X, Yang D, *et al.* A colloidal aqueous electrolyte modulated by oleic acid for durable zinc metal anode. Chem Eng J, 2023, 451: 138589
60 Zhang Y, Zheng X, Wu K, *et al.* Nonionic surfactant-assisted *in situ* generation of stable passivation protective layer for highly stable aqueous Zn metal anodes. Nano Lett, 2022, 22: 8574–8583
61 Geng Y, Miao L, Yan Z, *et al.* Super-zincophilic additive induced interphase modulation enables long-life Zn anodes at high current density and areal capacity. J Mater Chem A, 2022, 10: 10132–10138
62 Jin Y, Han KS, Shao Y, *et al.* Stabilizing zinc anode reactions by polyethylene oxide polymer in mild aqueous electrolytes. Adv Funct Mater, 2020, 30: 2003932
63 Yang J, Zhang Y, Li Z, *et al.* Three birds with one stone: Tetramethylurea as electrolyte additive for highly reversible Zn-metal anode. Adv Funct Mater, 2022, 32: 2209642

Acknowledgements This work was financially supported by the National Natural Science Foundation of China (52271222, 51902301 and 22379096), the Natural Science Foundation of Zhejiang Province (LY21E020006), and Shanghai Science and Technology Commission (21010503100 and 23DZ1202500).

Author contributions Chen T and Zheng S proposed the idea; Shen Q conducted the experiments; Shen Q and Li X performed the data analysis; Shen Q and Chen T wrote the paper with support from Pang Y and Zheng S; Xia S and Yuan T contributed to the theoretical analysis. All authors contributed to the general discussion.

Conflict of interest The authors declare that they have no conflict of interest.

Supplementary information Experimental details and supporting data are available in the online version of the paper.

Qibin Shen is currently a postgraduate student at the School of Materials and Chemistry, University of Shanghai for Science and Technology. His research interest mainly focuses on the aqueous electrolyte for zinc batteries.

Taiqiang Chen received his PhD from the East China Normal University. He is currently a lecturer at the School of Materials and Chemistry, University of Shanghai for Science and Technology. His research interests are in the development of advanced materials for batteries, including electrode materials, electrolytes and additives.

Shiyou Zheng received his BS, MS, and PhD degrees from Sichuan University, Zhejiang University, and Fudan University, respectively. He then became a visiting researcher at the National Institute of Standards and Technology and the University of Maryland. He is currently a professor at the University of Shanghai for Science and Technology. His research interests include new energy materials for batteries, supercapacitors, and hydrogen storage.

水系锌电池中自组装电极-电解质界面相实现高可逆的锌金属负极

沈琪彬[†], 陈泰强[†], 李馨, 夏水鑫, 袁涛, 庞越鹏, 郑时有[*]

摘要 由于缺乏先进的固体电解质界面相, 水系锌电池的循环寿命受到锌金属负极副反应和枝晶等问题的严重制约. 本文介绍了一种由两性分子(APMs)电解液添加剂构建而成的自组装电极-电解质界面相(AEEI). 作为一个示范, 这里选取聚乙烯吡咯烷酮(PVP)用做APMs, 因为它的羰基氧原子与芳香性的吡咯环共轭, 从而具有较强的电子给体性质. X射线光电子能谱和傅里叶变换红外光谱分析表明, AEEI的形成和稳定是由APMs的羰基氧原子同时与锌金属和锌离子相互作用推动的. 所形成的AEEI主要由富含锌离子的APMs致密层状胶束构成. 在电解质中保持APMs的含量在临界聚集浓度(~0.1%)以上, 可以保证AEEI的固有稳定性, 避免裂纹形成或脱落等问题. 得益于其抑制水分解副反应和不利的二维锌扩散的能力, 在AEEI的作用下实现了无枝晶的锌沉积. 在1 M $Zn(OTf)_2$添加1% PVP的电解液中, 形成的AEEI保证了锌对称电池具有超过2000小时的长循环寿命, Zn||Ti电池500个循环后库仑效率高于99.2%, 以及V_2O_5||Zn全电池500个循环后容量的高保持率(达76%).